Chemometrics and Intelligent Laboratory Systems 277 (2026) 105828

Contents lists available at ScienceDirect

Chemometrics and Intelligent Laboratory Systems

journal homepage: www.elsevier.com/locate/chemometrics

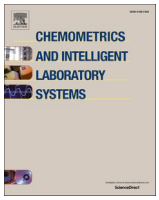

A chemometric approach to evaluating the mechanical properties of castable refractory ceramics for the aluminium foundry industry

Stefano Pezzoli [a,*], Stefano Scesa [a], Antonietta Lo Conte [b], Stefano Pierpaolo Marcello Trasatti [a]

[a] Department of Environmental Sciences and Policy, Università degli Studi di Milano, Milan, 20133, Italy
[b] Department of Mechanical Engineering, Politecnico di Milano, Milan, 20156, Italy

ARTICLE INFO

Keywords:
Aluminium
Refractory ceramics
Mechanical properties
Chemometrics

ABSTRACT

Chemometrics applies statistical and data-driven methods to design experiments and extract chemically-relevant information from multivariate datasets. In this study, chemometric modelling using the Chemometric Agile Tool (CAT) software was employed to quantify the influence of individual raw materials on the mechanical properties of an SiO_2-based castable refractory designed for aluminium-industry applications. Refractory ceramics are essential in aluminium production due to their thermal stability and mechanical integrity under high-temperature compressive loads, which ensures dimensional control and longer service life during molten aluminium handling. Accordingly, the mechanical properties of twenty-two formulations were evaluated by systematically varying raw material proportions around a commercial reference mixture to generate a comprehensive experimental domain. Specimens were prepared and tested in accordance with ASTM standards C133-97 and C674-13 to evaluate compressive and three-point flexural strengths. Compressive strength testing emerged as the most reliable indicator for this material class, and a multiple linear regression (MLR) model quantified the contribution of each raw material to cold crushing strength. The MLR results explained over 90% of the variance in the completed datasets, revealing the positive influence of the cementitious portion and specific fused silica fractions, as well as the complex role of colloidal silica and boron nitride. Moreover, increased total water content showed a negative correlation with compressive strength, likely due to higher porosity and defect formation. Finally, recommendations for formulation strategies and further property evaluation and optimisation are provided, demonstrating the value of Design of Experiments (DoE) in industrial formulation development.

1. Introduction

Aluminium's central role in modern industry and society stems from its favourable combination of abundance, low density, corrosion resistance, durability and a wide range of mechanical properties thanks to its ease of alloying. The industrial-scale extraction of aluminium via the Hall-Héroult electrolytic process, developed independently by Charles Martin Hall and Paul Héroult in the late 19th century, underpins the continued growth of global production. Due to its increasing industrial relevance, primary aluminium output rose from 6800 metric tonnes in 1900 to 73,009,000 metric tonnes according to the most recent data available for 2024 [1]. Furthermore, aluminium's cost- and energy-convenient recyclability, combined with negligible degradation during recycling, contributes to the circular economy and sustainability efforts. Casting is a foundational technique for fabricating aluminium-based products across several industries, such as automotive, aerospace, construction and infrastructure, packaging, telecommunications and electronics. Various casting techniques are employed depending on the application-specific requirements. In this context, recent studies on integrating aluminium casting processes have reported improvements in cracking and porosity-related issues [2].

Casting and melt-handling in aluminium manufacturing require specialised equipment capable of withstanding prolonged exposure to the material in its molten state and therefore made from appropriate materials or mixtures, such as ceramics, sand or a high-melting-point metals [3]. This is where castable refractory ceramics play a critical role by simplifying the mould-making process as these products are prepared as liquid slurries that retain the given shape after drying. In

* Corresponding author.
E-mail addresses: stefano.pezzoli@unimi.it (S. Pezzoli), stefano.scesa@studenti.unimi.it (S. Scesa), antonietta.loconte@polimi.it (A. Lo Conte), stefano.trasatti@unimi.it (S.P.M. Trasatti).

https://doi.org/10.1016/j.chemolab.2026.105828
Received 9 February 2026; Received in revised form 11 June 2026; Accepted 18 July 2026
Available online 20 July 2026

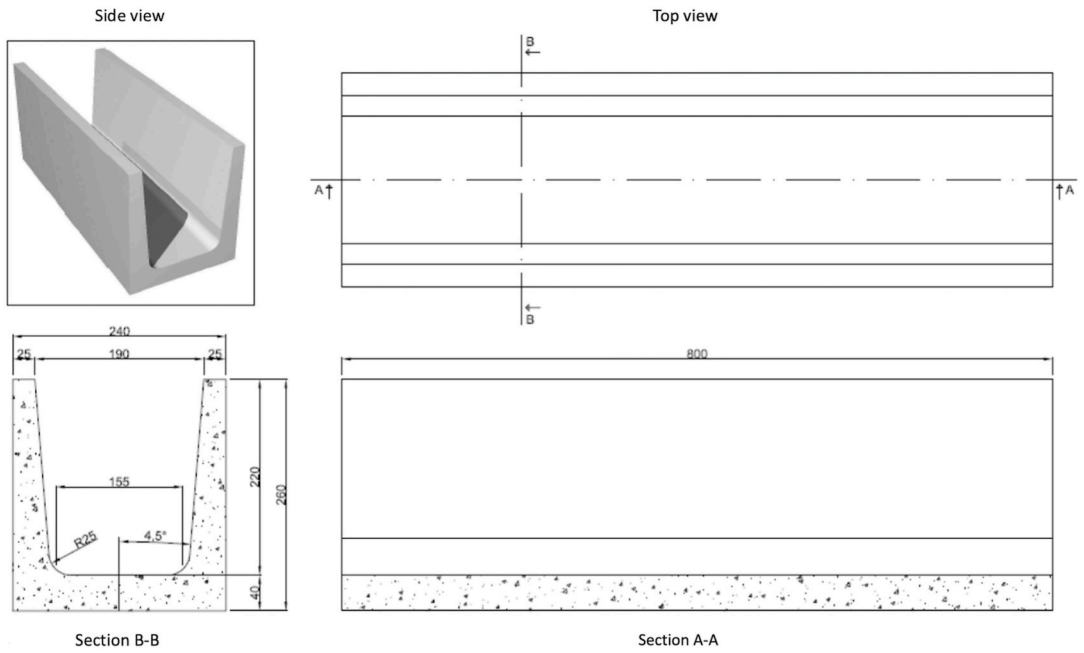

Fig. 1. *Geometry and views of the ceramic component.* Illustration (side view) and technical drawings (top and sectional views) of a channel-like component, representing one of the main categories of commercial ceramic products used in the aluminium industry. This specific component was designed, fabricated, and commercialised by the partner company, and its formulation serves as the reference material for this study.

addition to metal shaping, refractories are used to line the interiors of melting and holding furnaces, and to fabricate components for equipment designed to transport molten aluminium. Due to the extreme environment caused by the direct and prolonged contact with molten aluminium, these products must exhibit high-temperature stability, thermal shock resistance, chemical resistance and mechanical strength, while also providing formability, durability and insulating properties. Their performance relies heavily on a complex interplay between chemical composition and microstructural features. Failures in SiO_2--based refractories typically arise from chemical attack by aluminium alloys, thermal damage, microstructural degradation and mechanical fracture. Schurecht and Sephton [4] published one of the earliest academic articles on the interaction between molten aluminium and ceramics in 1940, observing an increase in the strength of fired bricks as a result of an aluminothermic reaction between the metal and silica in clay and grog at 930 °C. Subsequently, scientific research in this field expanded rapidly. In 1953, Brondyke [5] observed that all commercial alumina-silica refractories were unable to resist aluminium corrosion because of their wettability and penetrability, highlighting for the first time the problem of silicon pickup as impurity in aluminium baths. More recently, Afshar et al. [6] evaluated the performance of various aluminosilicates under prolonged exposure to molten aluminium, finding that high-alumina content (>99%) showed increased corrosion resistance. In contrast, refractories rich in silica, iron oxide and alkali metal oxides (Na_2O, K_2O) exhibited significant corrosion. Éntin et al. [7] highlighted the advantages of andalusite components for anode-firing kilns over Russian mullite-based refractories due to their higher thermal and chemical stability and mechanical properties. Additionally, they developed low-cement refractories with enhanced resistance to aluminium-driven corrosion by using calcium hexaaluminate (CA_6) as an anti-wetting agent, replacing baryte, whose environmental impact is linked to its ability to release volatile sulphurous compounds upon decomposition. Calcium hexaaluminate (CA_6) was also used by Hemrick et al. [8] in the development of one of two high-corrosion resistance industrial ceramic products, the other being an alumina-silicon carbide composite. Finally, studying modern aluminium production, which incorporates various alloying elements, is crucial for determining how these elements affect the properties of the ceramics involved in the processes. Reichert et al. [9] recently revealed that Zn and Mg penetrate refractories differently, inducing extensive microstructural changes. Zinc primarily forms gahnite ($ZnAl_2O_4$) when reacting with alumina-based ceramics under oxidising conditions due to ZnO formation, while magnesium generates $MgAl_2O_4$ spinels under inert conditions.

SiO_2-based refractories belonging to the family of channel-like systems, namely launders, were investigated in this study (Fig. 1). Among the physical, thermal and mechanical properties characterising these materials, mechanical behaviour is particularly important as it is often associated with industrial non-conformities. The mechanical resistance of ceramic products is strongly influenced by both raw material selection and the manufacturing process, especially microstructure features such as porosity and the tendency for microcrack formation during sintering. Furthermore, these advanced refractory components must withstand significant thermo-mechanical loads during service. Consequently, compressive strength and three-point flexural strength are key parameters for assessing the operational lifetime and reliability of these ceramic products. Owing to the multifunctional nature of the raw materials and processing parameters, a univariate optimisation strategy is inadequate as it fails to capture the interactions between variables. Chemometric analysis offers a robust, data-driven framework to address this complexity through structured experimental designs that systematically explore composition-processing space.

2. Experimental section

2.1. Aim of the work

In this work, screening designs and multiple linear regression (MLR) models were employed to quantify the influence of each raw material on the final ceramic's mechanical properties and to prioritise variables for subsequent response-surface DoE optimisation. Compressive and three-point flexural strengths served as the primary evaluation metrics. Because the manufacturing process involves several intricate steps – including mixing of solid and liquid components, staged drying in wooden moulds and in air, and subsequent high-temperature sintering – this study focuses exclusively on quantifying the effects of the raw

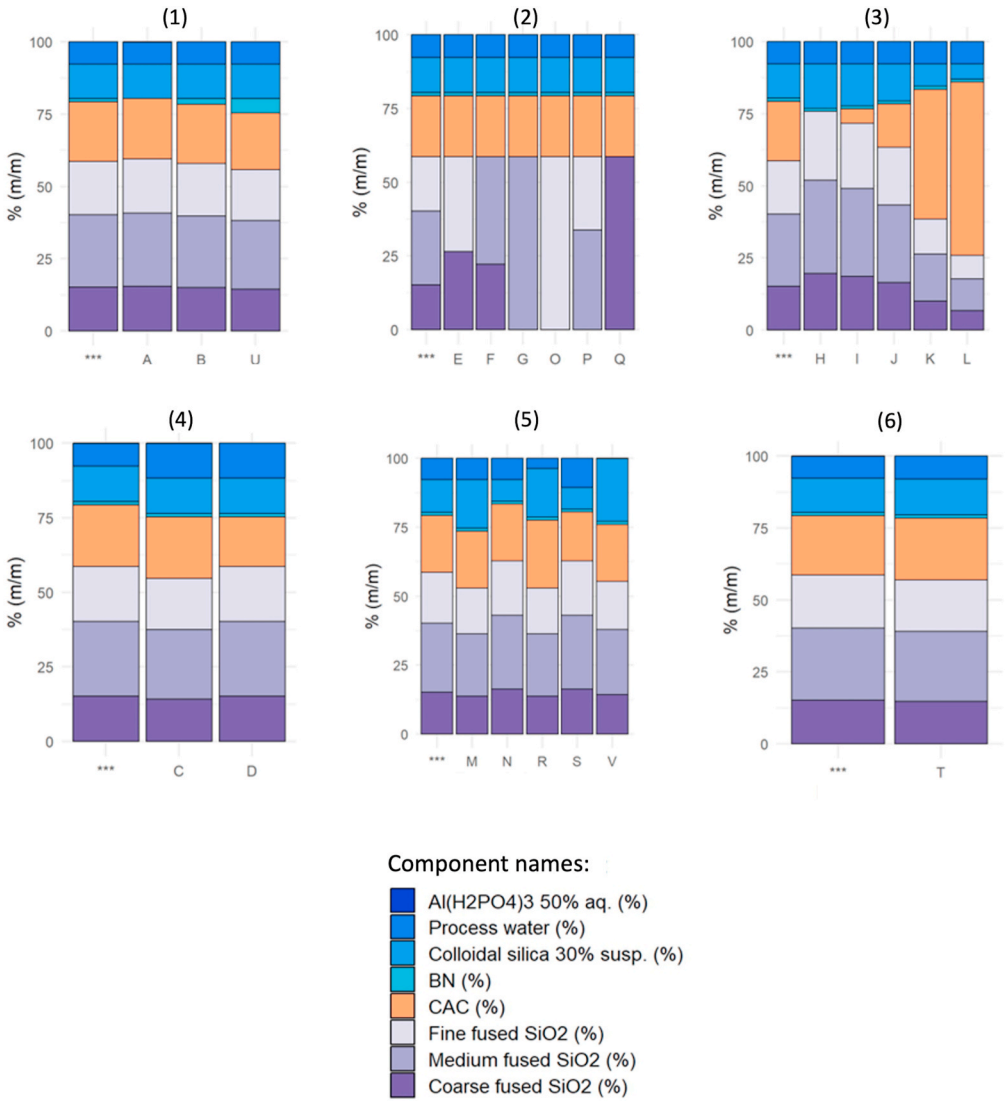

Fig. 2. *Composition of designed formulations.* Histogram representation of all designed formulations, each identified by a corresponding letter. Coloured bars indicate the contribution of each raw material. Formulations are organised into purposeful groups, namely: (1) BN concentration series, (2) fused silica granulometry variations, (3) CAC/fused silica ratio series, (4) water content variation, (5) increased colloidal silica series, and (6) minor compositional variations.

materials on the mechanical resistance properties. The investigation integrates two complementary analyses into a single, coherent framework, using a screening set of twenty formulations (labelled A–T), supplemented by two additional formulations (U and V) to broaden the experimental domain. While twenty-two formulations reflect a substantial effort within an industrial screening context, the relatively high number of compositional variables results in a constrained observation-to-variable ratio. To address potential limitations related to model stability and overfitting, the analysis was complemented by statistical diagnostics, ensuring the robustness and reliability of the regression results within the investigated compositional domain.

2.2. Materials

The castable refractory ceramic consisted of three fused silica fractions (coarse, medium and fine granulometries), a calcium aluminate cementitious (CAC) component, hexagonal boron nitride (h-BN or BN), a 30% suspension of colloidal silica in water, a 50% aqueous solution of aluminium dihydrogen phosphate, and process water. The main properties of each raw material and their role in the formulation are briefly summarised below.

2.2.1. Fused silica

Fused silica is an amorphous form of silicon dioxide (SiO_2) with a unique combination of chemical, thermal and mechanical properties. It is produced by melting high-purity quartz at high temperatures, followed by rapid cooling to prevent crystallisation. Its low density, high mechanical strength, thermal shock resistance, corrosion resistance and low cost make fused silica ideal for industrial applications [10].

2.2.2. Calcium aluminate cement (CAC)

Calcium aluminate cements (CACs) are a special class of cements predominantly used in high-temperature applications. CACs differ from ordinary Portland cement due to the absence of silica and a high alumina (Al_2O_3) content, typically ranging from 40 to 80%. Alumina and calcium oxide (CaO) are sintered to form calcium aluminate phases. CAC reacts with water through two main stages [11,12]. First, the anhydrous powder solubilises, and subsequently, hydrated phases precipitate as elongated crystals. Furthermore, the type of hydrated compounds formed depends on the curing temperature and the cement composition [11]. In this study, a high-performance industrial-grade CAC with a nominal 70% Al_2O_3 content was employed.

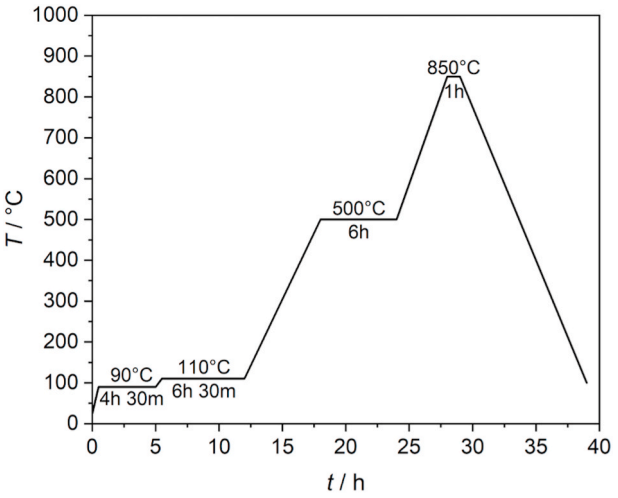

Fig. 3. *Sintering temperature-time profile.* Temperature-time profile of the sintering program applied to commercial products and laboratory specimens. The thermal cycle consists of four heating ramps and four dwell stages, followed by a cooling step. Temperature and dwell time at each plateau are indicated.

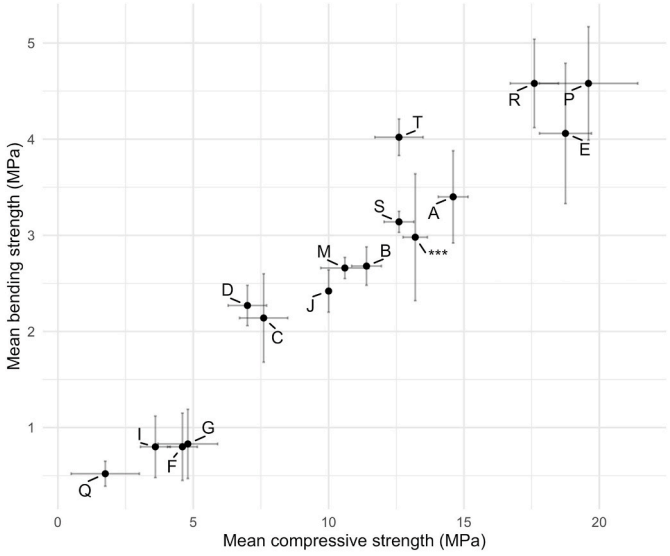

Fig. 4. *Relationship between compressive and bending strength.* Mean compressive strength versus mean bending strength for all initially tested formulations. Each point represents a formulation, and error bars indicate standard deviation for both properties.

2.2.3. Boron nitride

Boron nitride (BN) is a unique inorganic compound with extraordinary properties that make it highly valuable for a wide range of advanced materials. It can exist in both amorphous and crystalline forms, with the most common crystalline forms being hexagonal (h-BN) and cubic (c-BN), the former being more thermodynamically stable. Hexagonal boron nitride exhibits high thermal stability and conductivity, chemical inertness and a very high elastic modulus [13,14].

2.2.4. Colloidal silica

Colloidal silica is a stable dispersion of fine, amorphous and non-porous SiO_2 particles in a liquid, usually water. The solid particles generally range from 1 to 1000 nm in diameter, and their ability to remain suspended is due to the negative surface charge, which prevents aggregation. The well-known capacity of colloidal silica to act as a binder in ceramic materials is discussed by de Mendonça Spera et al. [15], who provide insights into the design and production of mullite-based ceramics, using colloidal silica as a binder to enhance mechanical and thermal properties. A commercially available 30% colloidal silica suspension in water was used in this research.

2.2.5. Aluminium dihydrogen phosphate

Aluminium dihydrogen phosphate ($Al(H_2PO_4)_3$) is an inorganic compound, soluble in water, that forms a strong and thermally stable bond when used in combination with ceramic materials [16]. Verweij et al. [17] investigated $Al(H_2PO_4)_3$ binding behaviour with quartz microspheres at different temperatures, highlighting its mechanisms. A 50% aqueous solution of $Al(H_2PO_4)_3$ was purchased directly from the market and its proportion remained constant in this chemometric study due to its relatively small percentage in the mixture (*ca.* 0.04%).

2.3. Formulation design and sample preparation

A screening test of twenty formulations, labelled from A to T, was prepared by varying the proportions of the aforementioned components around a commercial formulation, targeted as ***. The designed formulations were organised into purposeful groups to investigate specific factors: (1) BN concentration series; (2) fused silica granulometry variations; (3) CAC/fused silica ratio series; (4) water content variations (compensated either by fused silica or CAC); (5) variations in colloidal silica content, with or without normalised water additions; and (6) minor compositional variations. Two further formulations, U and V, were subsequently prepared to expand the experimental domain. Formulation U contained a higher BN content (5 wt%), while formulation V maximised colloidal silica content by supplying the entire liquid portion as colloidal silica suspension, without added process water. The designed formulations are shown in Fig. 2.

Specimens were prepared by thoroughly mixing the solid and liquid raw materials according to the proportions specified in each formulation. The resulting slurry was then poured into cubic (50 mm sides) and prismatic (10 mm × 25 mm × 115 mm) moulds, corresponding to the geometries required for compressive and flexural strength testing, in accordance with ASTM standards C133-97 [18] and C674-13 [19], respectively. The moulds were pre-coated with a mineral oil-based detaching agent to facilitate removal of the green bodies. The samples were initially left to air-dry for 30 min, removed from the moulds after hardening and dried under ambient conditions for several days to ensure the complete removal of free water. Finally, the dried materials were sintered in a Nabertherm P330 muffle furnace according to the controlled heating program illustrated in Fig. 3. The sintering ramp was designed to promote binder dehydration and densification while minimising thermal shock and cracking. At 90 °C, the objective is the gradual removal of free and capillary-bound water, decreasing steam pressure buildup within the green bodies, thereby reducing microcracking and warping. Prolonged holding at 110 °C ensures the complete removal of residual absorbed water trapped within fine pores, which is essential to prevent explosive spalling during subsequent heating stages. The dwell at 500 °C represents a critical step as it corresponds to the dehydration and decomposition of calcium aluminate hydrates, accompanied by the development of open porosity that facilitates the safe release of evolved water vapour. Finally, heating to 850 °C initiates the early sintering regime, promoting initial densification while preserving the controlled porosity required for thermal insulation and simultaneously avoiding the formation of critical crystalline silica phases such as cristobalite.

2.4. Mechanical testing

Mechanical testing at room temperature was performed in accordance with ASTM standards C133-97 for compressive strength and ASTM C674-13 for three-point flexural strength. Compressive strength tests were conducted using an MTS Alliance RF/150 Universal Testing Machine (UTM), and three-point flexural strength tests were carried out

Table 1
Mean compressive and bending strength results, with the relative pooled variance (σ_p^2) and coefficient of variation (*CV*) values for all tested formulations.

Compression test				Three-point bending test			
Formulation	Mean/MPa	σ_p^2/MPa^2	CV/%	Formulation	Mean/MPa	σ_p^2/MPa^2	CV/%
A	15	0.3	4	A	3	0.2	14
B	11	0.3	5	B	3	0.04	8
C	8	0.8	12	C	2	0.2	22
D	7	0.5	10	D	2	0.04	9
E	19	0.9	5	E	4	0.5	18
F	5	0.3	12	F	1	0.1	44
G	5	1.2	23	G	1	0.1	44
I	4	0.3	15	I	1	0.1	40
J	10	0	0	J	2	0.05	9
M	11	0.8	8	M	3	0.01	4
P	20	3.3	9	P	5	0.4	13
Q	2	1.6	72	Q	1	0.02	25
R	18	0.8	5	R	5	0.2	10
S	13	0.3	4	S	3	0.01	4
T	13	0.8	7	T	4	0.04	5
***	13	0.2	3	***	3	0.4	22

Note: *CV* = (standard deviation/mean) x 100. Bending CVs exceed compression CVs in 11 of 16 formulations; *mean CV* (compression) = 12%, *mean CV* (bending) = 18%; *median CV* (compression) = 8%, *median CV* (bending) = 14%.

using an MTS Synergy 200, both available at the Department of Mechanical Engineering, Politecnico di Milano. For each tested formulation, a minimum of five replicate specimens were prepared, and at least four of them were measured in both bending and compression tests to provide replicate statistics.

2.5. Chemometric analysis

A multiple linear regression (MLR) model was constructed to relate component mass fractions (regressors) to measured strength (response). Raw material fractions were expressed as mass percentages of the total formulation. In this work, the MLR model was built using R-script Chemometric Agile Tool (CAT) software [20]. Initial MLR (i-MLR) results were based on formulations A–T, while the updated model (u-MLR) included formulations U and V to evaluate the effect of domain expansion on coefficients and model fit. In both MLR models, the solid fraction of the 30% colloidal silica suspension was isolated from the aqueous phase to allow independent analysis of its specific contributions.

2.6. Statistical model validation and robustness analysis

To assess the reliability and stability of the updated multiple linear regression (u-MLR) model, a series of statistical diagnostics and validation procedures were implemented using the R programming language. Multicollinearity among the predictor variables was evaluated using the Variance Inflation Factor (VIF), which allows identification of potential linear dependencies. The VIF value associated with the *i-th* predictor measures the extent to which the variance of its regression coefficient is inflated due to correlations with other predictors and is defined as shown in Equation (2.1).

$$VIF_i = \frac{1}{1 - R_i^2} \quad \text{Eq. 2.1}$$

where R_i^2 is the R^2-value obtained by regressing the *i-th* predictor against all remaining predictors. Model adequacy was examined through residual diagnostics. In particular, the residuals-versus-fitted plot was inspected to evaluate homoscedasticity, while the normal probability plot of residuals was used to assess the assumption of normality of errors. Influential observations were identified using Cook's distance, which quantifies the effect of removing an individual observation on the estimated regression coefficients. Observations with Cook's distance exceeding the conventional threshold of $4/n$ (where n is the number of observations) were examined individually. Predictive performance was assessed using leave-one-out cross-validation (LOOCV), which provides an estimate of the model's generalisation capability. Model performance metrics included the root mean squared error of cross-validation (RMSECV) and the cross-validated coefficient of determination (Q^2). To account for replicate measurements, cross-validation was performed both at the specimen level and at the formulation-averaged level, providing complementary insights into predictive robustness. Finally, model stability was assessed using a bootstrap resampling approach. The dataset was resampled with replacement over 1000 iterations, and the u-MLR model was recalculated for each iteration (bootstrap sample). The resulting distributions of regression coefficients were used to evaluate coefficient variability, derive empirical confidence intervals, and assess the robustness of coefficient signs and magnitudes across resampled datasets.

2.7. Prediction uncertainty analysis

To quantify the uncertainty associated with model predictions, prediction intervals were computed for each specimen and formulation response. Unlike confidence intervals of regression coefficients, prediction intervals account for both parameter uncertainty and observations variability, providing a more realistic representation of the predictive reliability. Prediction intervals were calculated at a 95% confidence level and reflect the combined effect of model uncertainty and residual variance. The resulting intervals were visualised in parity plots to enable direct comparison between experimental and fitted values, while explicitly representing the uncertainty associated with each individual prediction.

3. Results and discussion

3.1. Castability and handling

Of the twenty initial designs, fifteen novel formulations were successfully castable and withstood handling for mechanical testing. The remaining formulations failed during processing due to insufficient workability or structural integrity. Formulations K, L and N were non-castable due to excessively low water-to-CAC ratios, resulting in unworkable mixtures. Moreover, formulation O, composed only of the fine fused silica fraction, disintegrated upon touch, indicating insufficient cohesion and demonstrating the need for coarser particles to obtain reasonable results. Finally, formulation H failed to attain adequate cohesion due to the absence of the cementitious phase (CAC), emphasising its role as a primary constituent in the system despite the presence of a colloidal silica binder. Additionally, formulations U and V did not

Table 2
Compressive and bending strength results and relative pooled variance (σ_p^2) values for all tested specimens.

Compression test			Three-point bending test		
Specimen	Result/MPa	σ_p^2/MPa^2	Specimen	Result/MPa	σ_p^2/MPa^2
A1	15	0.3	A1	3.8	0.2
A2	15		A2	3.4	
A3	14		A3	3.9	
A4	14		A4	2.7	
A5	15		A5	3.2	
B1	11	0.3	B1	2.5	0.04
B2	11		B2	3.0	
B3	11		B3	2.7	
B4	12		B4	2.7	
B5	12		B5	2.5	
C1	7	0.8	C1	2.7	0.2
C2	7		C2	2.4	
C3	9		C3	1.9	
C4	8		C4	1.5	
C5	7		C5	2.2	
D1	6	0.5	D1	2.5	0.04
D2	7		D2	2.0	
D3	7		D3	2.1	
D4	8		D4	2.2	
D5	7		D5	2.3	
			D6	2.5	
E1	18	0.9	E1	3.5	0.5
E2	20		E2	3.2	
E3	19		E3	4.1	
E4	18		E4	4.5	
E5	n.d.		E5	5.0	
			E6	4.2	
F1	5	0.3	F1	1.1	0.1
F2	4		F2	0.9	
F3	4		F3	1.0	
F4	5		F4	0.8	
F5	5		F5	0.2	
G1	6	1.2	G1	1.1	0.1
G2	6		G2	0.9	
G3	4		G3	0.3	
G4	4		G4	1.0	
G5	4		G5	n.d.	
I1	4	0.3	I1	0.9	0.1
I2	4		I2	1.0	
I3	4		I3	0.7	
I4	3		I4	0.3	
I5	3		I5	1.1	
J1	10	0	J1	2.6	0.05
J2	10		J2	2.6	
J3	10		J3	2.3	
J4	10		J4	2.5	
J5	10		J5	2.1	
M1	9	0.8	M1	2.5	0.01
M2	11		M2	2.6	
M3	11		M3	2.8	
M4	11		M4	2.7	
M5	11		M5	2.7	
P1	18	3.3	P1	4.2	0.4
P2	18		P2	5.4	
P3	22		P3	5.0	
P4	21		P4	4.3	
P5	19		P5	4.0	
Q1	3	1.6	Q1	0.4	0.02
Q2	2		Q2	0.6	
Q3	2		Q3	0.4	
Q4	0		Q4	0.7	
Q5	n.d.		Q5	0.5	
R1	18	0.8	R1	5.2	0.2
R2	18		R2	3.9	
R3	18		R3	4.6	
R4	18		R4	4.6	
R5	16		R5	4.6	
S1	12	0.3	S1	3.1	0.01
S2	13		S2	3.3	
S3	12		S3	3.2	
S4	13		S4	3.0	
S5	13		S5	3.1	
T1	14	0.8	T1	4.1	0.04
T2	12		T2	4.0	
T3	12		T3	3.9	
T4	12		T4	4.3	
T5	13		T5	3.8	
***1	13	0.2	***1	3.3	0.4
***2	13		***2	2.6	
***3	13		***3	3.4	
***4	13		***4	2.0	
***5	14		***5	3.6	

Note: "n.d." = non-determinable.

exhibit any castability or handling issues, bringing the total number of formulations effectively tested to seventeen, excluding the commercial reference.

3.2. Mechanical testing: bending versus compression

Across the first successfully tested formulations, flexural strength in three-point bending and compressive strength were found to be linearly correlated (Fig. 4). This relationship suggests that, within the investigated compositional window, similar microstructural features govern both tensile- and compressive-dominated failure modes. However, three-point bending exhibited greater variability and a number of premature failures at cross-sections far from the cross-section of maximum bending moment, which were not representative of the bulk material. Millimetric fused silica grains in the coarse fraction may have acted as local stress concentrators during the three-point bending test, therefore increasing scatter compared with compression. This trend is supported by a quantitative comparison of the coefficients of variation (CV), where bending strength showed higher dispersion than compressive strength in 11 out of 16 formulations (Table 1). Although not universal across all compositions, this indicates that flexural response is more sensitive to local microstructural defects. Based on these findings, compressive strength was selected as the primary response variable for subsequent modelling and screening analysis due to its lower variability and higher experimental robustness. Mean strength values and pooled variances for each formulation are summarised in Table 1, while Table 2 reports the individual compressive and bending strength measurements for all tested specimens.

3.3. Multiple linear regression (MLR) models

The experimentally observed formulation space is characterised by constrained compositional variability and inherent multicollinearity among raw material fractions. Because all components are expressed as mass fractions summing to unity, the system constitutes a classical mixture problem. However, although mixture-specific models (*e.g.*, Scheffé polynomials) were considered, a first-order multiple linear regression (MLR) model was adopted due to the limited dataset size and the primary goal of screening rather than optimisation. In fact, the objective of this approach is not to establish a fully general predictive model, but rather to identify dominant formulation trends and provide a

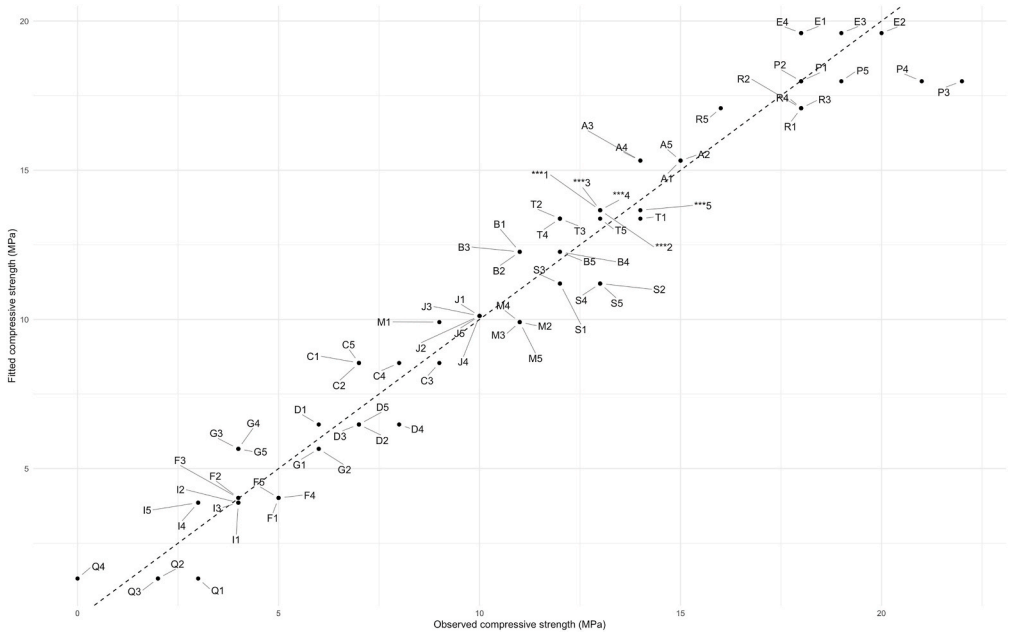

Fig. 5. *Fitted versus observed compressive strength (i-MLR).* Fitted compressive strength as a function of observed (experimental) values for the initial multiple linear regression (i-MLR) model. The dashed line represents the identity line (y = x).

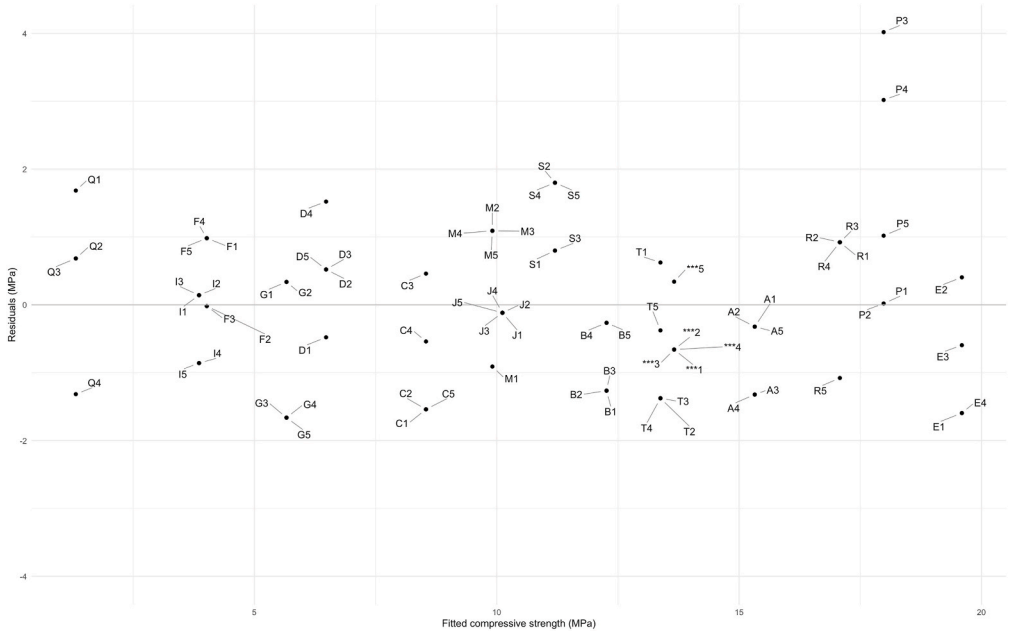

Fig. 6. *Residuals plot for the i-MLR model.* Residuals from the initial multiple linear regression (i-MLR) model plotted against fitted values. The grey line indicates zero residual level.

practical tool for formulation optimisation within the explored composition space. In this context, two complementary MLR models were developed, which were formulated without an intercept term to reflect the dependency of the component proportions and constraints imposed by mixture relationships.

3.3.1. Initial MLR (i-MLR) model

The initial multiple linear regression (i-MLR) model was built using the compressive strength test results of formulations A–T and the commercial formulation (***). This model explained 95% of the variance in compressive strength and exhibited a satisfactory agreement between observed (experimental) and fitted values (Fig. 5). The residuals-versus-fitted plot did not reveal any clear systematic patterns, suggesting that the linear approximation is adequate within the investigated compositional domain (Fig. 6). Residuals ranged from −1.66 to 4.02, with a median value of −0.07, indicating a distribution centred close to zero. Coefficient directions and significance in the i-MLR model are summarised in Fig. 7 and described as follows.

- Positive contributors: CAC, medium and fine fused silica fractions, and the solid portion of the colloidal silica suspension were associated with increases in compressive strength.
- Negative contributors: BN and total water content were linked to decreases in compressive strength.

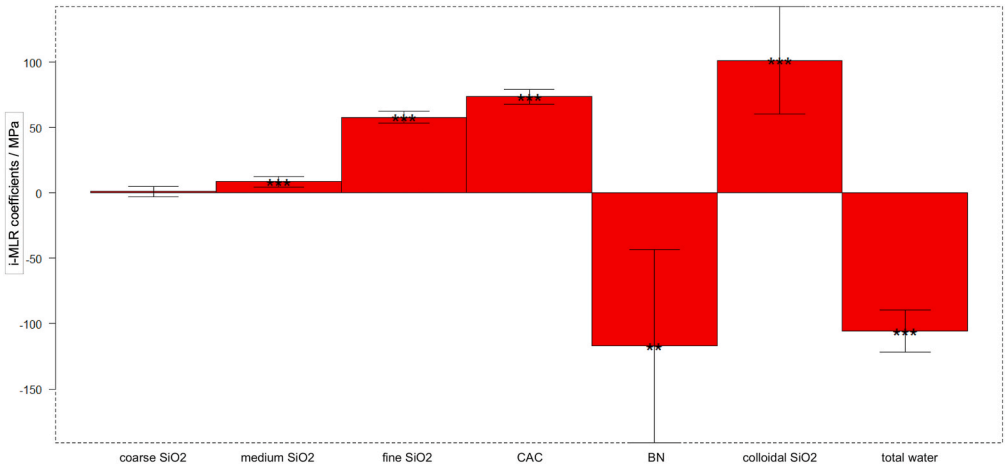

Fig. 7. *Regression coefficients of raw materials (i-MLR).* Estimated contributions of raw materials to the i-MLR model expressed as regression coefficients. Error bars represent coefficient uncertainty, and statistical significance is denoted by asterisks.

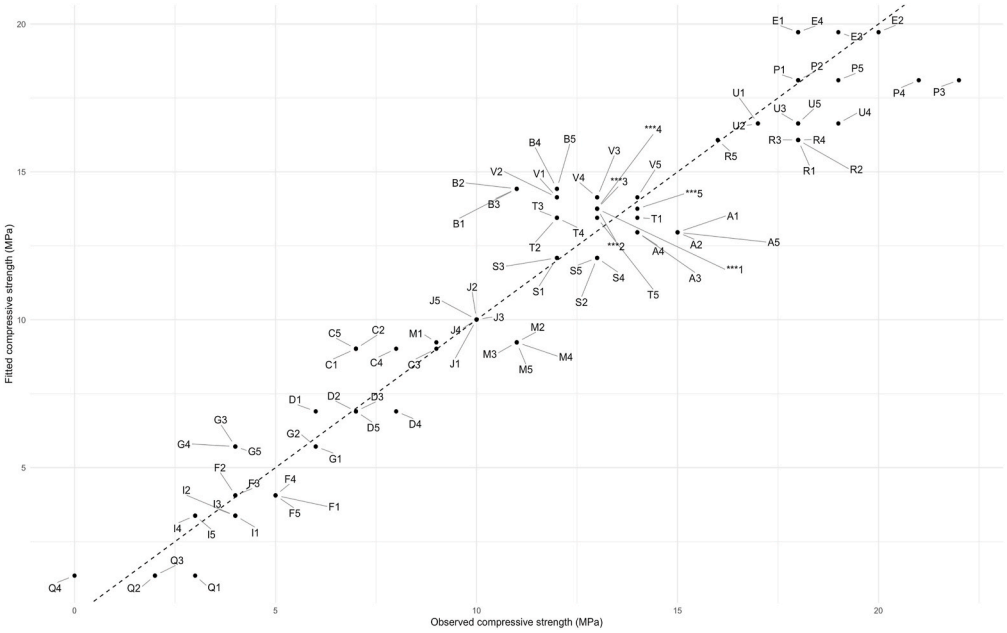

Fig. 8. *Fitted versus observed compressive strength (u-MLR).* Fitted compressive strength as a function of observed (experimental) values for the updated multiple linear regression (u-MLR) model. The dashed line represents the identity line (y = x).

- Insignificant contributors: the coarse fused silica fraction produced a non-statistically significant coefficient, indicating that its presence has no influence on compressive strength.

These trends suggest that, as expected, the cementitious component and certain finer fused silica fractions improve particle packing, thereby increasing compressive strength. In contrast, higher free water content and the addition of BN lubricant appear to reduce mechanical performance by promoting the formation of initial defects. In castable refractories, adding more water to the formulation mix improves initial flowability but leads to higher final porosity. As confirmed by previous studies, excess water leaves behind interconnected voids as it evaporates during drying, significantly reducing mechanical strength by limiting solid-to-solid contact and promoting crack initiation under load [21]. Moreover, Wang et al. [22] reported that BN nanosheets (BNNSs) and nano-sized BN (BNn) showed detrimental agglomeration in SiO_2-based refractories: their nanoscale dimensions facilitate defect initiation, ultimately impairing strength resistance properties.

3.3.2. *Updated MLR (u-MLR) model*

Two additional formulations, U and V, were introduced to explore regions of the experimental domain not covered by the previous model. The updated MLR (u-MLR) model explained 92% of the variance and maintained a reasonable agreement between experimental and fitted values (Fig. 8). Also in this case, no systematic patterns were detected in the residual diagnostic and residual values ranged from −3.43 to 3.90, with a median value of −0.01 (Fig. 9). While the effects of fused silica granulometries, CAC and total water remained consistent with the initial model, the signs and magnitudes of the coefficients for BN and colloidal silica changed, as illustrated in Fig. 10. In the u-MLR model, the BN content exhibited a positive correlation with compressive strength, suggesting its role as a strength-reinforcing phase within the investigated compositional range. This finding is consistent with recent literature indicating that appropriately dispersed BN particles can improve the mechanical resistance of silica-based ceramics by refining grain structure and promoting energy dissipation mechanisms [22]. The contrasting results between the two models likely reflect the

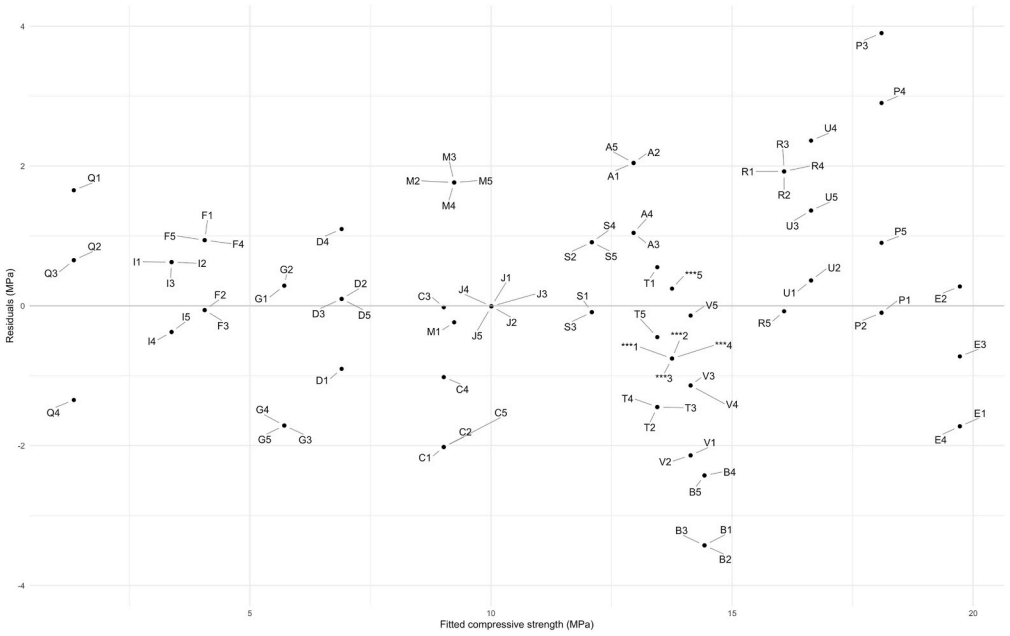

Fig. 9. *Residuals plot for the u-MLR model.* Residuals from the updated multiple linear regression (u-MLR) model plotted against fitted values. The grey line indicates zero residual level.

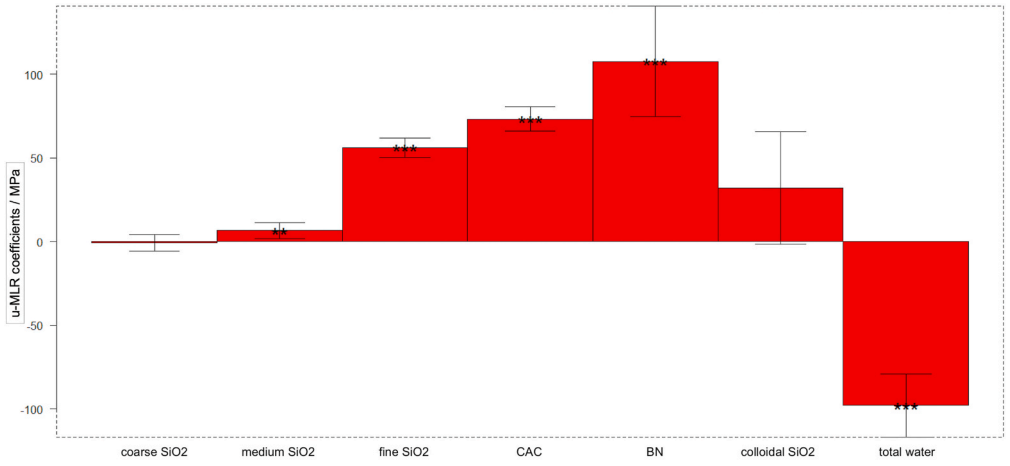

Fig. 10. *Regression coefficients of raw materials (u-MLR).* Estimated contributions of raw materials to the u-MLR model expressed as regression coefficients. Error bars represent coefficient uncertainty, and statistical significance is denoted by asterisks.

Table 3
Experimental domain and MLR coefficients for each raw material derived from the u-MLR model for compressive strength testing of SiO_2-based castable refractories.

Raw material	Experimental domain/ %	β (u-MLR coefficient)/ MPa
Coarse fused silica	0 – 59	-0.8 ± 2.5
Medium fused silica	0 – 59	6.7 ± 2.4
Fine fused silica	0 – 32	56.3 ± 2.9
Calcium Aluminate Cement (CAC)	5 – 25	73.4 ± 3.6
Boron nitride (BN)	0 – 5	107.8 ± 16.6
Colloidal silica	2 – 7	32.1 ± 17.0
Total water	16 – 20	-98.0 ± 9.5

Note: For u-MLR coefficients, positive values may indicate a positive contribution of the corresponding raw material to compressive resistance.

Table 4
Valence Inflation Factors (VIFs) of raw material predictors in the u-MLR model.

Raw material	VIF
Coarse fused silica	9.4
Medium fused silica	18.1
Fine fused silica	10.9
Calcium Aluminate Cement (CAC)	18.9
Boron nitride (BN)	2.8
Colloidal silica	18.3
Total water	98.0

domain-limited linearity and the competing effects of BN agglomeration versus microstructural reinforcement. The effect of boron nitride on compressive strength appears to be strongly dependent on the explored compositional domain and may be influenced by interaction and non-linear effects. In particular, the positive coefficient observed in the

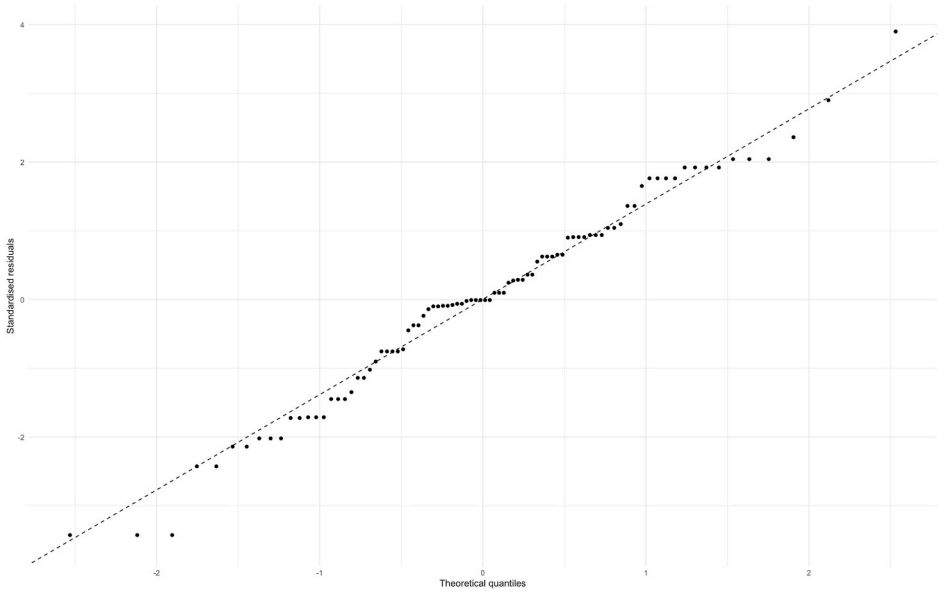

Fig. 11. *Normal probability plot of residuals (u-MLR).* Standardised residuals plotted against theoretical quantiles for the u-MLR model. The dashed line represents the theoretical normal quantiles.

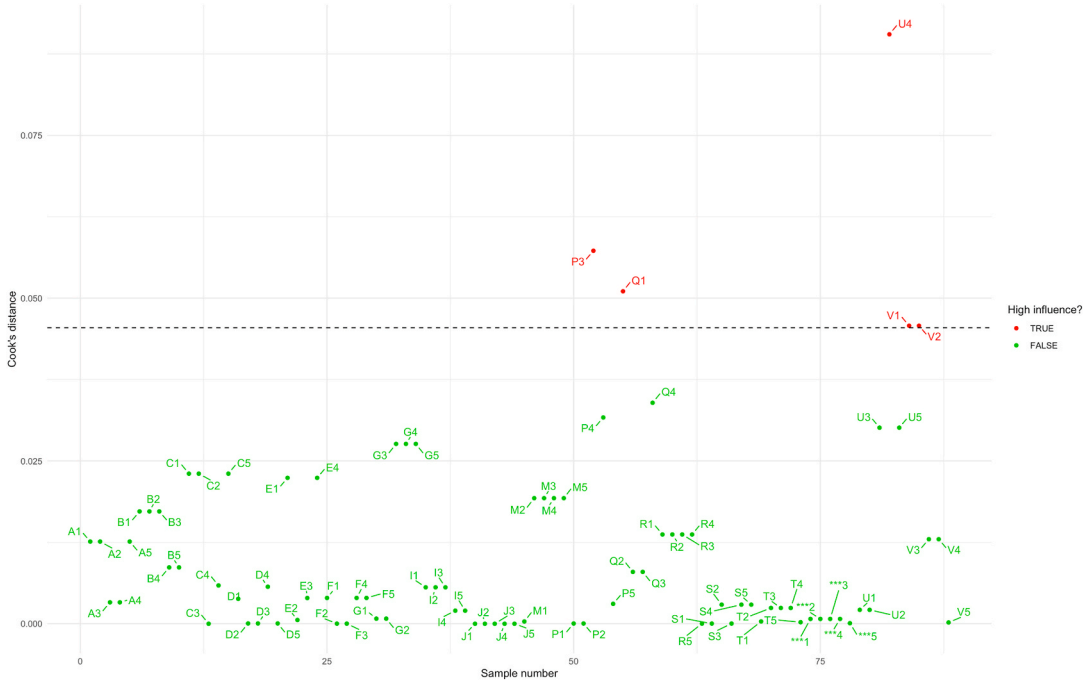

Fig. 12. *Cook's distance analysis.* Cook's distance plot for the complete dataset (n = 88). The dashed line represents the threshold of *4/n*, and observations exceeding this value are flagged as potentially influential.

u-MLR may be partially affected by leverage effects associated with the limited representation of high-BN compositions. Therefore, the contribution of BN should be interpreted cautiously as a composition-dependent effect rather than a universally positive or negative predictor of compressive strength. Similarly, the effect of colloidal silica was modified upon inclusion of formulation V, in which the entire liquid fraction was supplied via colloidal silica suspension. Across the full dataset, the solid fraction of the colloidal silica suspension showed no statistically significant effect.

Table 3 summarises the experimental domains and the coefficient values derived from the updated multiple linear regression (u-MLR) analysis for each raw material, highlighting their relative contributions to compressive strength. The resulting coefficients (β_i) can be incorporated into Equation 3.1 to estimate the cold crushing strength (CCS) of a novel formulation based on the mass fraction of each raw material. However, this relationship should be interpreted as a local empirical model valid only within the explored compositional domain. In fact, the model accounts only for first-order mixture effects and therefore does not enable the identification of a formulation with optimal compressive resistance. Despite this limitation, the study served as an initial screening test and provided valuable results and insights into the mechanical behaviour of SiO_2-based castable refractory ceramics for applications in the aluminium industry.

Table 5
Bootstrap statistics of the u-MLR regression coefficients (R = 1000 and CI = 95%).

Raw material	*u-MLR coefficients*			*Bootstrap coefficients (R=1000)*		
	β 2.5%/MPa	β/MPa	β 97.5%/MPa	β 2.5%/MPa	β/MPa	β 97.5%/MPa
Coarse fused silica	−5.8	−0.8	4.2	−6.6	−1.7	2.9
Medium fused silica	1.8	6.7	11.5	1.4	5.9	10.6
Fine fused silica	50.5	56.3	62.1	51.5	57.1	62.7
Calcium Aluminate Cement (CAC)	66.2	73.4	80.5	69.1	76.7	85.2
Boron nitride (h-BN)	74.8	107.8	140.8	56.6	94.3	118.7
Colloidal silica	−1.7	32.1	65.9	−5.0	26.6	68.6
Total water	−116.7	−98.0	−79.1	−117.6	−97.7	−77.6

$$CCS\ (MPa) = \beta_{coarse\ SiO_2} \cdot \frac{m_{coarse\ SiO_2}}{m_{TOT}} + \beta_{medium\ SiO_2} \cdot \frac{m_{medium\ SiO_2}}{m_{TOT}} + \beta_{fine\ SiO_2} \cdot \frac{m_{fine\ SiO_2}}{m_{TOT}} + \beta_{CAC} \cdot \frac{m_{CAC}}{m_{TOT}} + \beta_{BN} \cdot \frac{m_{BN}}{m_{TOT}} + \beta_{coll.\ SiO_2} \cdot \frac{m_{coll.\ SiO_2}}{m_{TOT}} + \beta_{H_2O} \cdot \frac{m_{H_2O}}{m_{TOT}}$$

Eq. 3.1

3.3.3. Limitations

The primary limitations of the developed MLR models stem from linearity assumptions and restricted domain coverage. Because MLR treats variable effects as purely additive and linear, any interactions between components are effectively neglected. The observed changes in coefficient signs upon inclusion of formulations U and V may suggest the presence of underlying interaction terms or non-linear dependencies beyond the scope of MLR. Additionally, incomplete domain coverage caused by non-castable or unstable formulations created unsampled regions and potential bias in the regression space.

3.4. Regression model diagnostics

The experimental campaign produced a total of 88 compressive strength measurements, corresponding to replicate specimens prepared across 18 distinct formulations. Following the development of the u-MLR model, diagnostic analyses were performed and the results are shown as follows.

Variance Inflation Factor (VIF) analysis was employed to quantify multicollinearity among the predictor variables describing raw material composition. As expected, the results indicate severe multicollinearity for several predictors, with elevated VIF values for most constituents (Table 4). This behaviour may arise from the experimental design constraints of the mixture system rather than from redundant variable specification. In particular, the three silica granulometries were varied while maintaining proportional relationships, calcium aluminate cement (CAC) content was adjusted as a function of total silica, and water content was coupled to CAC to ensure specimen workability and minimum compressive strength requirements. Consequently, strong dependencies are structurally embedded in the dataset. In contrast, boron nitride (BN) exhibited comparatively lower multicollinearity due to its partially independent variation within a limited experimental domain. Due to these results, further evaluation analyses were carried out.

Key assumptions of linear regression were evaluated through residual diagnostics. As already mentioned, no systematic patterns were observed, as the residuals were centred close to zero for both MLR models, indicating homoscedasticity (Figs. 6 and 9). Moreover, the normal probability plot of residuals for the u-MLR model shows a close alignment with the theoretical normal distribution, with points distributed approximately along the diagonal and only minor deviations observed at the distribution tails, indicating that the assumption of normality is reasonably satisfied (Fig. 11).

Cook's distance was computed to evaluate the influence of individual observations on the fitted regression model. Using a threshold of 4/n

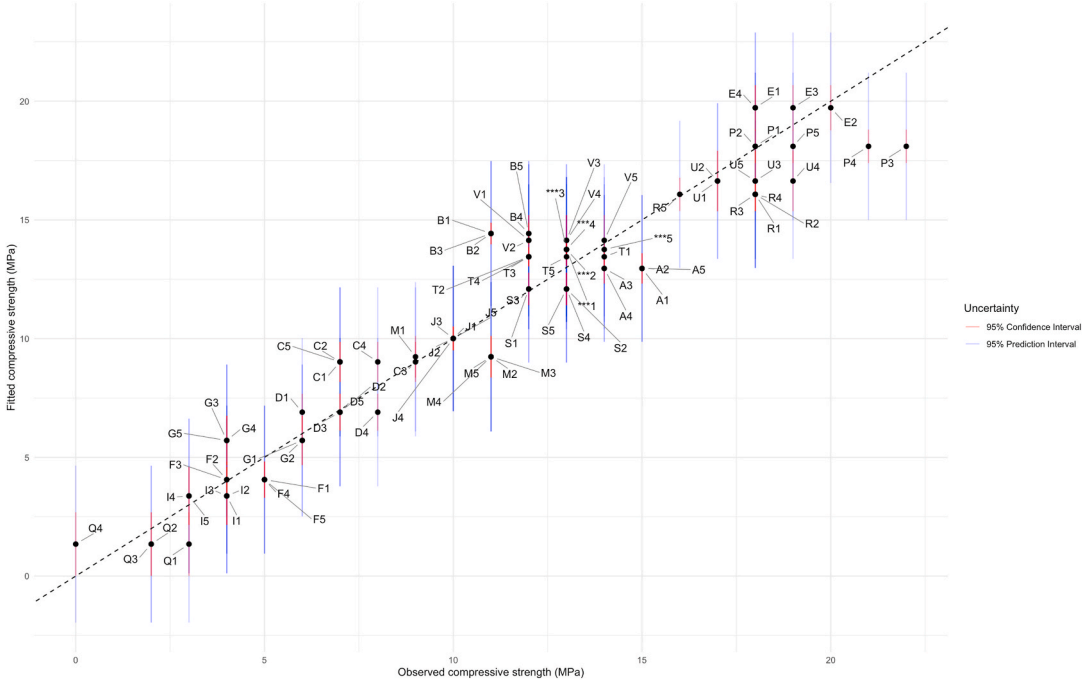

Fig. 13. *Parity plot at specimen level.* Measured versus fitted compressive strength for the u-MLR model at the specimen level. The dashed line represents the identity line (y = x). Error bars indicate 95% confidence intervals (in red) and 95% prediction intervals (in blue).

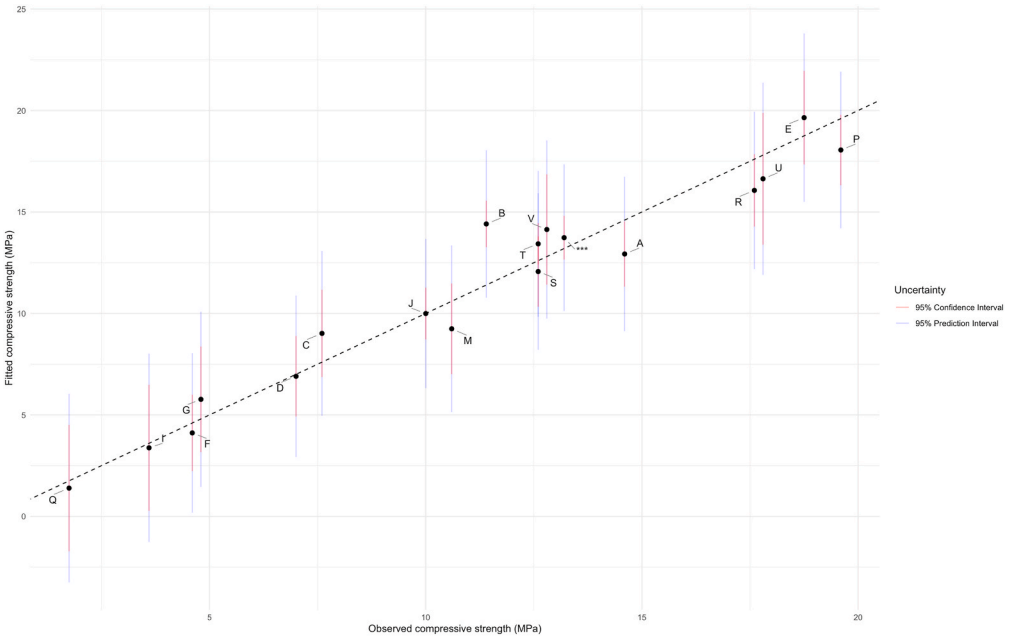

Fig. 14. *Parity plot at formulation level.* Measured versus fitted compressive strength for the u-MLR model at the formulation level. The dashed line represents the identity line (y = x). Error bars indicate 95% confidence intervals (in red) and 95% prediction intervals (in blue).

(where n = 88), five observations exceeded this criterion indicating potentially influential data points (Fig. 12). These observations correspond to formulations U and V, as well as Q and P. The specimens associated with formulations U and V were produced under different environmental conditions (*e.g.*, variations in humidity and temperature during fabrication), which may have influenced the measured response. On the other hand, formulations Q and P correspond to extreme response values, representing the minimum and maximum measured compressive strengths, respectively. All observations were retained, as they correspond to physically meaningful conditions within the experimental domain.

The stability and uncertainty of the u-MLR coefficients were assessed using bootstrap resampling with 1000 iterations, and the results are reported in Table 5. The bootstrap analysis is consistent with the original model coefficients, indicating good model stability. For most variables, both the sign and magnitude of the coefficients are preserved, with relatively small deviations. Fine fused silica and CAC exhibit strong and stable positive effects, while total water consistently shows a strong negative contribution. Medium fused silica remains positive and relatively stable. In contrast, coarse fused silica and colloidal silica exhibit wider uncertainty, with confidence intervals approaching or including zero, suggesting weaker or less certain effects. Boron nitride remains positively associated with compressive strength but shows greater variability between bootstrap iterations, reflecting its limited coverage within the compositional domain. Overall, the bootstrap analysis supports the robustness of the u-MLR model while highlighting increased uncertainty for minor components. This behaviour is particularly evident for BN, whose coefficient variability is consistent with the limited coverage of high-BN compositions.

To further evaluate the predictive reliability and generalisation capability of the u-MLR model, cross-validation was performed. Given the limited size of the dataset, leave-one-out cross-validation (LOOCV) was selected, as it maximises the use of available data in each iteration while providing a low-bias estimate of predictive performance. Model performance was assessed using the root mean squared error of cross-validation (RMSECV) and the cross-validated coefficient of determination (Q^2). For the complete dataset (n = 88), the model achieved an RMSECV of 1.57 MPa and a Q^2 of 0.910. The small difference between R^2 and Q^2 indicates that the model does not suffer from significant overfitting and retains strong predictive capability within the investigated compositional domain. However, since four to five replicate specimens were tested for each formulation, this validation approach may overestimate predictive performance due to the presence of correlated observations. To address this limitation, compressive strength values were averaged at the formulation level, and LOOCV was repeated on the aggregated dataset. Under these conditions, RMSECV and Q^2 values of 3.05 MPa and 0.704 were obtained, respectively. These results provide a more realistic estimate of predictive performance, as they better reflect the model's ability to generalise across distinct formulations rather than replicate measurements.

3.5. Predictive uncertainty and model applicability

Parity plots at both specimen and formulation levels show good agreement between observed and fitted compressive strength (Figs. 13 and 14). The associated confidence and prediction intervals provide a quantitative representation of the uncertainty in both the estimated mean response and individual predictions.

Overall, the results confirm that the u-MLR model provides reliable predictive performance within the investigated compositional domain. Although VIF values associated with certain predictors are relatively high, this primarily affects coefficient interpretability rather than predictive capability. The combined evidence from bootstrap analysis and cross-validation demonstrates that the model remains robust for prediction within the defined design space, while maintaining appropriate uncertainty bounds for predictions at the formulation level.

3.6. Effect of specific formulation modifications

To increase the water content, one major solid constituent was reduced at a time. In formulation C, total fused silica was decreased from 58.7 to 54.7 wt%, while in formulation D, the CAC level was lowered from 20.6 to 16.6 wt%. Both formulations exhibited a marked deterioration in mechanical performance compared with the reference sample, with compressive strength reductions up to 30–40%. This decline was attributed to increased porosity and crack formation resulting from higher water content, as confirmed by SEM analysis (Fig. 15a and b, compared with Fig. 15c). SEM analyses were carried out using a JSM

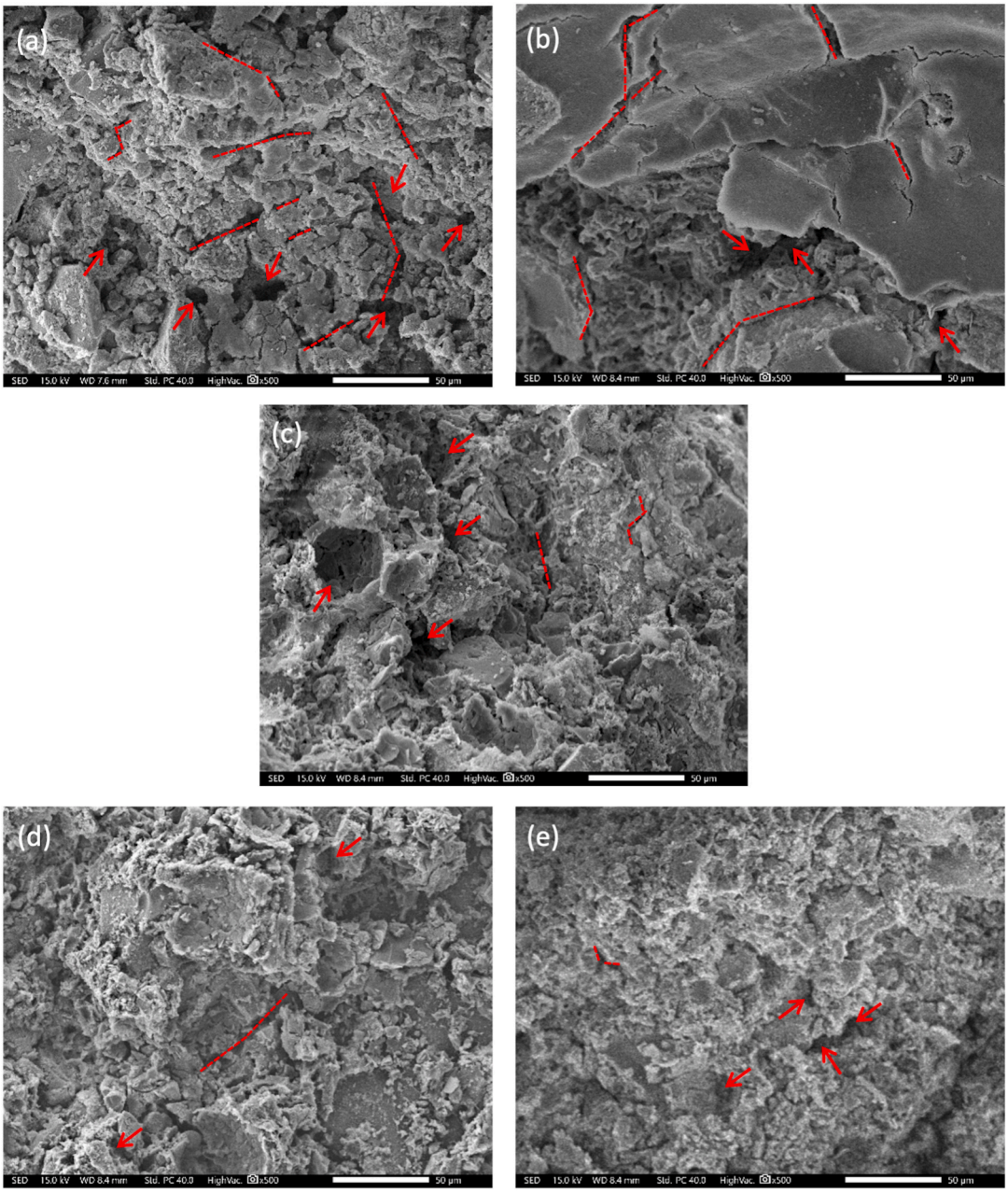

Fig. 15. *SEM microstructure of selected formulations.* SEM images of formulations (a) C, (b) D, (c) reference, (d) P, and (e) R. Images were captured at 500× magnification under high vacuum after gold coating. The scale bar represents 50 μm; red arrows and dashed lines highlight pores and micro-cracks, respectively.

IT500 LA scanning electron microscope (JEOL) equipped with a tungsten filament and operated under high-vacuum conditions. The analysed samples were coated with a thin gold layer using a SCANCOAT SIX coater (Edwards) to ensure adequate electrical conductivity. Furthermore, formulation E omitted the medium-fused-silica fraction, while formulation P excluded the coarser fraction. Additionally, in formulation R, the colloidal-to-fused silica ratio was adjusted from 1:5 to 1:3, with a corresponding increase in CAC content to rebalance the mixture. Formulations E, R and P exhibited improvements in mechanical properties of approximately 20%, 40% and 40% relative to the reference, respectively. Notably, formulations P and R demonstrated enhanced compressive and flexural strengths, along with a more compact microstructure (Fig. 15d and e, compared with Fig. 15c). Finally, quantitative XRD analysis did not reveal any clear correlation between the amorphous content or phase-to-phase ratios and the measured mechanical performance. XRD patterns were collected using an APD 2000 Pro diffractometer (GNR) equipped with a Cu-Kα radiation source over a 2θ range of 3–65° with a step of 0.02°. Data refinement was performed employing the Rietveld method with PROFEX software coupled to the BGMN calculation engine.

4. Conclusions

This work evaluated a series of SiO_2-based castable refractories formulated for applications in molten aluminium handling, using chemometric tools to quantify the effect of individual raw materials on mechanical performance. By integrating a systematic formulation strategy with statistical modelling, the approach enabled a mechanistic interpretation of compositional effects on compressive strength, a key indicator of structural integrity and service reliability for this material class. Compressive strength evaluation on 50 mm cubic specimens was identified as the most robust and reproducible screening metric,

outperforming three-point bending tests in sensitivity and consistency.

The multiple linear regression (MLR) analysis explained over 90% of the variance in compressive strength across the tested formulations. Positive contributions were associated with the cementitious component (CAC) and specific fused silica fractions (medium and fine fused silicas). In contrast, the coarse fused silica fraction exhibited an insignificant linear coefficient; however, its presence is necessary to prevent material disintegration, suggesting a threshold or percolation-driven effect that was not captured by simple additive terms. The effects of boron nitride (BN) and colloidal silica were more complex and dependent on the dataset. Boron nitride, valued for its lubricious and thermal properties, likely exerted non-linear or interaction-driven influences, possibly linked to dispersion or agglomeration. The positive coefficient observed for BN in the extended model suggests potential benefits at specific concentrations, highlighting the need for targeted factorial studies. Similarly, the solid component of the colloidal silica aqueous suspension improved green strength through particle bridging but affected final strength depending on its impact on packing, water balance, and subsequent bonding reactions. However, limited coverage at higher BN and colloidal silica contents may introduce extrapolation uncertainty, which may affect coefficient stability.

Future optimisation should incorporate non-linear modelling approaches and mixture-specific experimental designs to better capture interactions and mitigate multicollinearity among compositional variables. Furthermore, the effects of both processing conditions and high-temperature treatments should also be evaluated. Extensive evaluations of interparticle bonding, porosity, and pore size distribution would also provide more detailed insights into the mechanisms behind strength changes.

In conclusion, this study demonstrated that chemometric modelling combined with compressive strength testing provides a powerful framework for guiding formulation design in the refractory ceramics sector. The integration of Design of Experiments (DoE) principles with statistical analysis enables the rapid identification of key formulation drivers and accelerates the development of high-performance SiO_2-based castable refractories for the aluminium industry.

Funding sources

This work was supported by the European Union-Next Generation EU funds, PNRR: Mission 4 - Education and Research, Component 2 - From Research to Business, Investment 2.3 - Strengthening and thematic and territorial extension of technology transfer centres by industry segments. Implementing Body: MADE S.C.A R.L., 20133 Milan, Italy [grant No. H49J23001400008].

CRediT authorship contribution statement

Stefano Pezzoli: Conceptualization, Data curation, Formal analysis, Investigation, Methodology, Software, Writing – original draft, Writing – review & editing. **Stefano Scesa:** Conceptualization, Data curation, Formal analysis, Investigation, Methodology, Software. **Antonietta Lo Conte:** Conceptualization, Funding acquisition, Project administration, Resources, Supervision, Validation, Writing – review & editing. **Stefano Pierpaolo Marcello Trasatti:** Conceptualization, Funding acquisition, Project administration, Resources, Supervision, Validation, Writing – review & editing.

Declaration of competing interest

Prof. Stefano P. M. Trasatti had a Coordinated and Continuous Collaboration (Co.co.co.) with Foundry Ecocer S.r.l., while holding a part-time permanent position at the Università degli Studi di Milano at the time of this study. The company had no role in the design of the study, in the collection, analysis, or interpretation of the data, in the writing of the manuscript, or in the decision to publish the results. The other authors declare no competing financial interests or personal relationships that could have influenced the work reported in this paper.

Acknowledgments

The authors thank Dr. Stefania Crespi (Department of Earth Science "Ardito Desio", Università degli Studi di Milano) for performing SEM analyses and Dr. Francesco Dellisanti (Analitica S.a.s) for conducting quantitative XRD analyses. The authors gratefully acknowledge the partner company, particularly the staff of the ceramic department, and Dr. Matteo Labò and Mr. Maurizio Sala for their valuable support.

Data availability

Data will be made available on request.

References

[1] International Aluminium Institute, Primary aluminium production. https://international-aluminium.org/statistics/primary-aluminium-production/, 2024. (Accessed 20 January 2026).
[2] D. Li, C. Slater, H. Cai, X. Hou, Y. Li, Q. Wang, Joining technologies for aluminium castings—A review, Coatings 13 (2023) 958, https://doi.org/10.3390/coatings13050958.
[3] R. Lumley, Fundamentals of Aluminium Metallurgy: Production, Processing and Applications, Woodhead Pub, 2011.
[4] H.G. Schurecht, H.I. Sephton, Use of aluminum metal in the ceramic industry I, properties of refractories produced with mixtures of aluminum, fire clay, and grog, J. Am. Ceram. Soc. 23 (1940) 259–264, https://doi.org/10.1111/j.1151-2916.1940.tb14272.x.
[5] K.J. Brondyke, Effect of molten aluminum on alumina-silica refractories, J. Am. Ceram. Soc. 36 (1953) 171–174, https://doi.org/10.1111/j.1151-2916.1953.tb12860.x.
[6] S. Afshar, C. Allaire, The corrosion of refractory aggregates by molten aluminum, JOM 52 (2000) 43–46, https://doi.org/10.1007/s11837-000-0034-z.
[7] S.V. Éntin, G.S. Rossikhina, N.S. Mamonova, New refractory materials for the aluminum industry, Refract. Ind. Ceram. 47 (2006) 98–100, https://doi.org/10.1007/s11148-006-0065-2.
[8] J.G. Hemrick, W.L. Headrick, K.M. Peters, Development and application of refractory materials for molten aluminum applications, Int. J. Appl. Ceram. Technol. 5 (2008) 265–277, https://doi.org/10.1111/j.1744-7402.2008.02213.x.
[9] W. Reichert, D. Kenn, V. Sannikow, T. Tonnesen, R. Telle, Influence of modern aluminium alloys on the reaction behavior of refractory linings, IJCES 4 (2022) 180–185, https://doi.org/10.1002/ces2.10129.
[10] J.-K. Guo, J. Li, H.-M. Kou, Advanced ceramic materials, in: R. Xu, Y. Xu (Eds.), Modern Inorganic Synthetic Chemistry, Elsevier, 2017, pp. 463–492, https://doi.org/10.1016/B978-0-444-63591-4.00017-3.
[11] H.F.W. Taylor, Cement Chemistry, Academic Press, London, 1990.
[12] E. John, B. Lothenbach, Cement hydration mechanisms through time – a review, J. Mater. Sci. 58 (2023) 9805–9833, https://doi.org/10.1007/s10853-023-08651-9.
[13] S.N. Perevislov, Structure, properties, and applications of graphite-like hexagonal boron nitride, Refract. Ind. Ceram. 60 (2019) 291–295, https://doi.org/10.1007/s11148-019-00355-5.
[14] R. Haubner, M. Wilhelm, R. Weissenbacher, B. Lux, Boron nitrides — properties, synthesis and applications, in: M. Jansen (Ed.), High Performance Non-oxide Ceramics II, 2002, pp. 1–45.
[15] N.C. de Mendonça Spera, L. Fernandes, J. Sakihama, I. Santos Martinatti, P. Tiba, R. Salomão, Designing colloidal silica-bonded porous structures of in-situ mullite for thermal insulation, InterCeram Int. Ceram. Rev. 69 (2020) 54–63, https://doi.org/10.1007/s42411-020-0120-x.
[16] W.D. Kingery, Fundamental study of phosphate bonding in refractories: i, literature review, J. Am. Ceram. Soc. 33 (1950) 239–241, https://doi.org/10.1111/j.1151-2916.1950.tb14171.x.
[17] H. Verweij, G. De With, D. Veeneman, Hollow glass microsphere composites: preparation and properties, J. Mater. Sci. 20 (1985) 1069–1078, https://doi.org/10.1007/BF00585751.
[18] Standard Test Methods for Cold Crushing Strength and Modulus of Rupture of Refractories, C1vols. 33–97, ASTM, 2021, https://doi.org/10.1520/C0133-97R21.
[19] Standard Test Methods for Flexural Properties of Ceramic Whiteware Materials C6vols. 74–13, ASTM, 2018, https://doi.org/10.1520/C0674-13R18.
[20] R. Leardi, C. Melzi, G. Polotti, CAT (Chemometric agile tool), freely downloadable from. http://gruppochemiometria.it/index.php/software.
[21] A.P. Luz, M.H. Moreira, M.A.L. Braulio, C. Parr, V.C. Pandolfelli, Drying behavior of dense refractory ceramic castables. Part 1 – general aspects and experimental techniques used to assess water removal, Ceram. Int. 47 (2021) 22246–22268, https://doi.org/10.1016/j.ceramint.2021.05.022.
[22] W. Wang, J. Chen, X. Sun, G. Sun, Y. Liang, J. Bi, Mechanical properties and microstructure of hot-pressed silica matrix composites, Materials 15 (2022) 3666, https://doi.org/10.3390/ma15103666.